HIF isoforms in the skin differentially regulate systemic arterial pressure

Andrew S. Cowburn[a,b,c], Norihiko Takeda[c], Adam T. Boutin[c], Jung-Whan Kim[c], Jane C. Sterling[b], Manando Nakasaki[c], Mark Southwood[d], Ananda W. Goldrath[c], Colin Jamora[c], Victor Nizet[e], Edwin R. Chilvers[b,1], and Randall S. Johnson[a,1]

Departments of [a]Physiology, Development and Neuroscience and [b]Medicine, University of Cambridge CB2 3EG, Cambridge, United Kingdom; [d]Papworth Hospital, National Health Service Foundation Trust, Cambridge CB23 3RE, United Kingdom; [c]Division of Biological Sciences, Department of Pediatrics and [e]Skaggs School of Pharmacy and Pharmaceutical Sciences, University of California, San Diego, La Jolla, CA 92093

Edited by Gregg L. Semenza, The Johns Hopkins University School of Medicine, Baltimore, MD, and approved September 15, 2013 (received for review April 17, 2013)

Vascular flow through tissues is regulated via a number of homeostatic mechanisms. Localized control of tissue blood flow, or autoregulation, is a key factor in regulating tissue perfusion and oxygenation. We show here that the net balance between two hypoxia-inducible factor (HIF) transcription factor isoforms, HIF-1α and HIF-2α, is an essential mechanism regulating both local and systemic blood flow in the skin of mice. We also show that balance of HIF isoforms in keratinocyte-specific mutant mice affects thermal adaptation, exercise capacity, and systemic arterial pressure. The two primary HIF isoforms achieve these effects in opposing ways that are associated with HIF isoform regulation of nitric oxide production. We also show that a correlation exists between altered levels of HIF isoforms in the skin and the degree of idiopathic hypertension in human subjects. Thus, the balance between HIF-1α and HIF-2α expression in keratinocytes is a control element of both tissue perfusion and systemic arterial pressure, with potential implications in human hypertension.

HIF-alpha | arginase | vascular tone

Autoregulation of vascular flow in peripheral tissues is essential both for controlling local tissue perfusion and for the regulation of systemic blood pressure. This dual role for peripheral blood flow is dependent in turn on a range of factors that act to adjust local vascular tone. A key element of this control is the balance between O_2 demand and O_2 supply (1). This balance causes increased need for oxygen to induce increased blood flow. This regulatory pathway in peripheral tissues has a direct impact on systemic arterial pressure, because peripheral vascular resistance in large part determines total vascular resistance in the arterial bed.

The skin contains a very extensive series of vascular plexi. This vascular bed has a range of essential functions, which include regulating body temperature. Skin circulation also is altered in a number of disease states, including renal disease (2), hypercholesterolemia (3), peripheral vascular disease (4), heart failure, and hypertension (5). Identification of structural alterations to the subcutaneous microvasculature provides a powerful prognostic tool to predict cardiovascular events in hypertensive patients (6), and impaired microvascular vasodilation and capillary rarefaction is associated with familial predisposition to hypertension (7).

The heterodimeric transcription factors hypoxia-inducible factor-alpha (HIF-1α) and HIF-2α are essential for the maintenance of cellular oxygen homeostasis (8). In response to hypoxia, stabilized HIF-1α and HIF-2α proteins initiate the expression of genes that alleviate hypoxic stress, including genes promoting cell growth, adhesion, and migration, new vessel formation, and the development of vascular networks (9, 10).

Recent data from a number of groups have indicated that HIF-1α and HIF-2α can act in a dualistic manner to regulate a range of responses in vivo; these interactions include functionally opposing interactions with the Myc transcription factors (11–13), with the tumor suppressor p53(14-16), and with mTOR (17).

Work by Prabhakar and co-workers (18–20) showed that HIF-1α and HIF-2α global heterozygosity influenced ventilatory rates and thus a number of responses to oxygenation controlled by the carotid body. They now have extended this work to show that there also is a functional antagonism between the HIF isoforms that regulate cardiorespiratory homeostasis through the carotid body and adrenal medulla (21). This work connects HIF isoform balance and the global control of response to physiological oxygenation.

We have shown previously that in macrophages, nitric oxide (NO) homeostasis can be regulated differentially through the opposing transcriptional effects of Th1 and Th2 cytokines on HIF-1α and HIF-2α, respectively (22). NO is a key regulator of vascular tone (23), and the physiological importance of NO in the regulation of blood pressure is highlighted by the fact that pharmacological inhibition of NO synthases leads to severe hypertension (24).

Here we perform a detailed analysis of the role that HIF isoform balance plays in the regulation of nitric oxide equilibrium in the skin. Our results indicate that this balance in oxygen-responsive transcription factor isoforms is a key factor in the overall maintenance of systemic arterial pressures and that an alteration in this balance correlates with idiopathic hypertension in human subjects.

Results

To characterize how HIF might function as a modulator of NO and thereby influence tissue vascular autoregulation, with the skin as a model peripheral tissue, we used mouse strains with conditional alleles of the relevant HIFα isoforms crossed to mouse strains expressing Cre recombinase under the control of the keratin 14 (K14) promoter. This experimental platform drives the excision of the HIFα isoforms only where the K14 promoter is active, i.e., within basal layers of the epidermis. Of interest, keratinocyte deletion of HIF-2α induced greater HIF-1α stability in the skin than seen in WT controls, possibly suggesting some sort of compensatory mechanism. This phenomenon was

Significance

The differential expression of the hypoxia-inducible factor-alpha (HIF-α) isoforms in the skin of mice influences vascular resistance and is correlated with homeostatic regulation of nitric oxide synthesis. A correlation between HIF isoform expression and hypertension was found in skin biopsies from human subjects, and may indicate a mechanism in the etiology of idiopathic hypertension.

Author contributions: A.S.C., N.T., A.T.B., E.R.C., and R.S.J. designed research; A.S.C., A.T.B., J.-W.K., J.C.S., M.N., M.S., and R.S.J. performed research; A.S.C. contributed new reagents/analytic tools; A.S.C., N.T., A.T.B., A.W.G., C.J., V.N., E.R.C., and R.S.J. analyzed data; and A.S.C., A.W.G., E.R.C., and R.S.J. wrote the paper.

The authors declare no conflict of interest.

This article is a PNAS Direct Submission.

[1]To whom correspondence should be addressed. E-mail: rsj33@cam.ac.uk. or erc24@cam.ac.uk.

This article contains supporting information online at www.pnas.org/lookup/suppl/doi:10.1073/pnas.1306942110/-/DCSupplemental.

not observed in the K14cre-HIF-1α mice with regards to HIF-2α expression (Fig. S1).

HIF-1α has a key role in NO synthase 2 (NOS2) regulation in response to Th1 cytokines (25–27), and, as shown previously, HIF-2α has a similarly important role in the regulation of arginase-1 in a Th2-cytokine–dependent fashion (22). In macrophages HIF-1α–dependent expression of NOS2 results in increased NO, via increased L-arginine utilization, whereas depletion of L-arginine via enhanced arginase activity stimulated by HIF-2α induction of the arginase-1 gene acts to reduce available L-arginine. This alternative utilization of L-arginine reduces the availability of this substrate for NO synthases and thus indirectly reduces NO production (22).

To determine whether this pattern of differential HIF-1α/HIF-2α regulation of NO homeostasis also occurs in keratinocytes independently of cytokine stimulation, we analyzed both RNA (Fig. 1*A*) and protein (Fig. 1*B*) isolated from skin biopsies of K14cre-HIFα mice. These biopsies show markedly reduced expression of NOS2 mRNA and protein in K14cre-HIF-1α mice as compared with littermate controls. In contrast, K14cre-HIF-2α mice show marked reduction in the expression of both arginase-1 and -2 mRNA and protein (Fig. 1 *A* and *B* and representative Western blots in Fig. S2*A*).

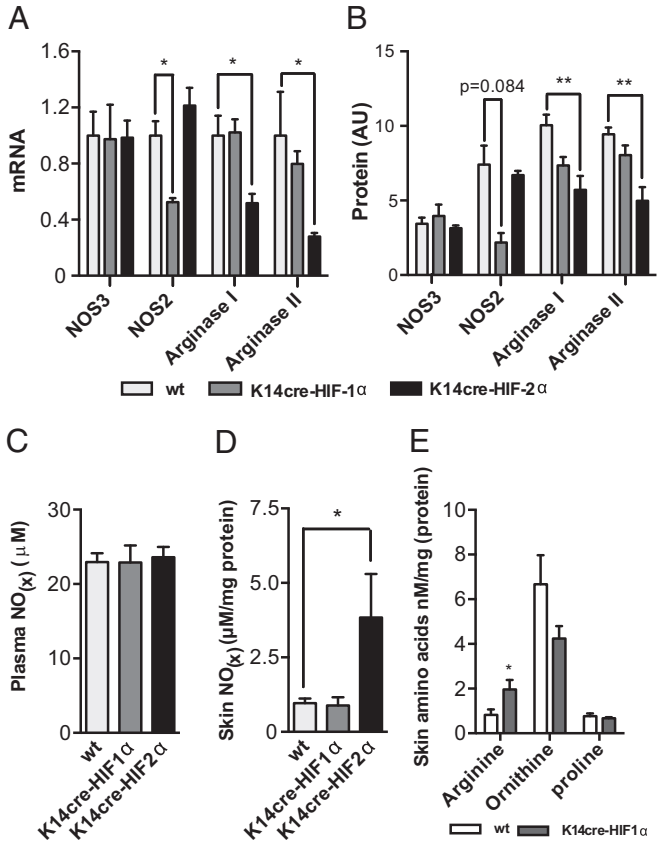

Fig. 1. Molecular and cellular characterization of mice with keratinocyte-specific deletion of HIF-1α or HIF-2α. (*A* and *B*) Baseline qPCR (*A*) and Western blot analysis (*B*) of HIFα target genes expressed in skin samples from keratinocyte-specific HIF-1α– (gray bar), or HIF-2α– (black bar) deleted mice compared with WT controls (open bars). Data are shown as mean fold change ± SEM for qPCR and mean protein arbitrary units (AU) ± SEM for Western blots ($n = 8$). (*C* and *D*) Baseline NOx analysis in plasma (*C*) and skin samples (*D*) from the K14cre-HIF-1α, K14cre-HIF-2α, and WT control mice described in *A* and *B*. Data are shown as mean ± SEM ($n = 9$). (*E*) Analysis of the soluble amino acid fraction in skin extracts from K14cre-HIF-1α mice ($n = 3$) compared with WT controls ($n = 3$). $^*P < 0.05$, $^{**}P < 0.005$.

Although analysis of plasma nitrates revealed little variation in basal concentrations between mutant mice and their littermate controls (Fig. 1*C*), measurement of skin nitrate levels revealed that K14cre-HIF-2α mutant mice accumulated far greater concentrations of nitrates than littermate controls (0.96 μM for control animals and 3.83 μM for K14cre-HIF-2α mutant mice, $n = 9$, $P < 0.05$) or K14cre-HIF-1α mutants (0.88 μM, $n = 9$) (Fig. 1*D*). Mass spectrometric analysis of free soluble amino acids extracted from the skin of K14cre-HIF-1α mice showed a significant increase in arginine (with nonsignificant changes in ornithine and proline), suggesting alterations in arginine utilization in the skin of these mice (Fig. 1*E*). Another prominent NOS, NOS1, appeared to be have a minimal level of expression in skin, and its expression was unaffected in the mutants (Fig. S2*B*). Together these observations indicate that the HIF pathway is a significant regulator of arginine utilization through known HIF targets such as NOS2/inducible NOS (iNOS).

Initial histological analysis suggested a normal development of skin architecture, with no abnormalities in the development of dermal blood vessels in any of the K14cre-HIF-α mutant mice compared with nontransgenic littermate controls (Fig. S3*A*), even though VEGF gene expression trended lower in K14cre-HIF1-α mice (Fig. S3*B*). Quantification identified a vascular density of 2.5–3% across the mutant and control animals (Fig. 2*A*). However, microvascular diameters were reduced significantly in the K14cre-HIF-1α mutant mice as compared with littermate controls (Fig. 2*B* and Fig. S3*C*).

Loss of epidermal HIF-1α did not affect either core body or skin temperatures; however, loss of HIF-2α significantly increased both core body (WT 37.05 ± 0.09 °C, HIF-2α mutant 37.47 ± 0.06 °C, $P < 0.005$, $n = 15$–29) and skin temperatures (WT 34.62 ± 0.22 °C, HIF-2α mutant 35.35 ± 0.10 °C, $P < 0.05$, $n = 17$–33) compared with WT littermate controls (Fig. 2 *C* and *D*). Furthermore, loss of epidermal HIF-2α significantly increased basal metabolism relative to that of littermate controls or K14cre-HIF-1α mice (Fig. S4 *A* and *B*).

Given the effects of deletion of the HIF-α isoforms on skin and core temperatures, a temperature-conservation challenge was used to determine whether the mechanisms for the preservation of core body temperature in the cold were affected in these mutants. K14cre-HIF-2α mice quickly became hypothermic relative to littermate control mice, with a significant defect in acclimation evident 3 h after the onset of cold stress (4 °C) (WT 35.5 °C, $n = 9$; HIF-2α mutant 34.6 °C, $n = 6$; $P < 0.05$) (Fig. 2*E*). Epidermal deletion of HIF-1α did not influence acclimation to cold environmental temperatures. There was a significant difference between the two isoform-knockout animals; again, each deviated from the WT core temperature in opposing directions.

To probe heat dissipation through the skin further and to determine whether HIF isoforms in keratinocytes had opposing effects on this vital physiological process, control and mutant mice were subjected to strenuous exercise during which significant defects in attaining a high $VO_{2\ max}$ were observed in both HIF-1α and HIF-2α keratinocyte mutants (Fig. S4 *C* and *D*). If this inability to attain a high VO_{2max} was caused by defects in heat dissipation through the skin (28), a higher core temperature should result from defective vasodilation, and a lower core temperature should result from excessive cutaneous vasodilation. Indeed, as shown in Fig. 2*F*, loss of cutaneous HIF-1α resulted in a significant elevation of core temperature after exercise relative to WT controls (WT 37.51 ± 0.21 °C, mutant 37.96 ± 0.08 °C, $P < 0.05$, $n = 6$). Furthermore, thermo-imaging before and after exercise revealed lower skin temperatures in the tails of K14cre-HIF-1α mice after exercise than seen in littermate controls (Fig. 2 *G* and *H*). These data indicate that the loss of either HIF-1α or HIF-2α in keratinocytes affects the systemic adaptive mechanisms required for heat dissipation, again in opposing fashions.

As a key negative regulator of HIFα protein stability, the tumor suppressor Von Hippel–Lindau factor (VHL) was examined for its effects on heat dissipation. Interestingly, in these mutants, the resultant increase in the expression of both HIF isoforms

PHYSIOLOGY

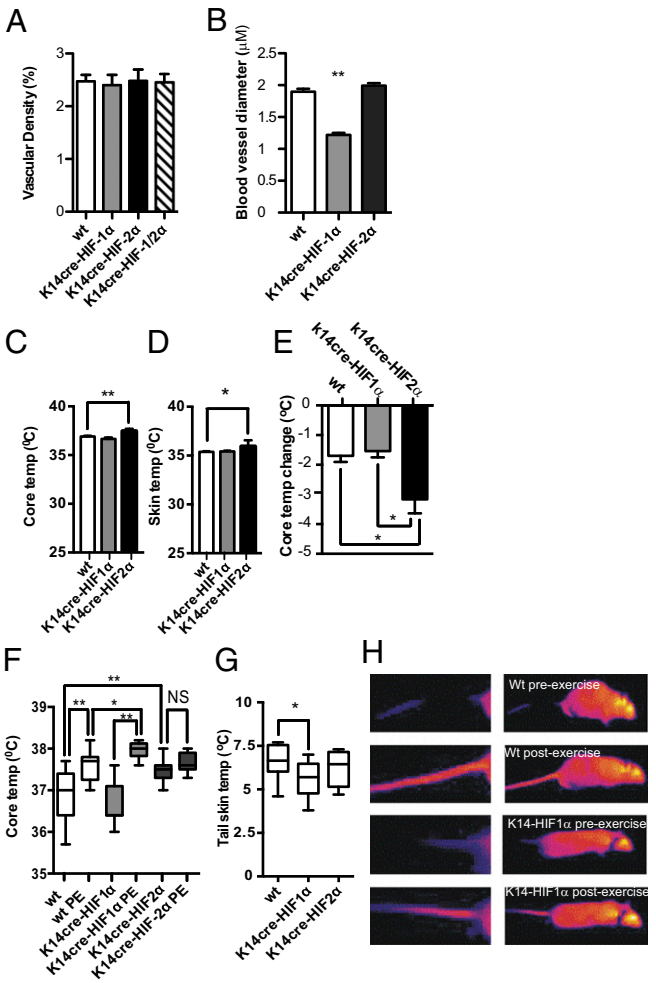

Fig. 2. Keratinocyte-specific deletion of HIFα influences skin vascular diameter and thermoregulation. (*A*) Histological analysis of vascular density; ImageJ software was used for quantitative analysis to determine the percentage vessel density. Sections from 10- to 12-wk-old K14cre-HIF-1α, K14cre-HIF-2α, and K14cre-HIF-1α/HIF-2α mice were analyzed and compared with nontransgenic littermate controls ($n = 4$). Data are shown as the percentage of CD31-positive staining ± SEM (*B*) Histological analysis of vascular diameter. ImageJ software was used for quantitative analysis to determine the vessel cross-section. Sections from K14cre-HIF-1α and K14cre-HIF-2α mice were analyzed and compared with nontransgenic littermate controls ($n = 4$), Data are shown as mean vessel diameter ± SEM. (*C* and *D*) Basal core body (*C*) and skin (*D*) temperature were analyzed in K14cre-HIF-1α, -HIF-2α, and WT mice (data are shown as mean °C ± SEM, $n = 15$–33). (*E*) Core body temperature was monitored during acclimation of K14cre-HIF-1α and K14cre-HIF-2α mice to an environmental temperature of 4 °C and was compared with WT controls. Data are shown as mean drop in core temperature (°C) ± SEM following 3-h exposure ($n = 6$–9). (*F*) Core body temperature (°C) was measured before and after exercise to determine the dissipation of heat ($n = 6$). (*G* and *H*) Tail-skin temperature was monitored before and after exercise stress. Thermal infrared imaging suggested that HIF-1α mutant mice dissipate significantly less thermal energy through the tail skin than WT mice. Data are shown as mean (°C) ± SEM ($n = 5$). *$P < 0.05$, **$P < 0.005$.

resulted in mice with greatly reduced skin temperatures (Fig. S5 *A*–*C*) as well as profound defects in adaptation to cold challenge and metabolism (Fig. S5 *D* and *E*).

One of the most important measures of alterations in peripheral vascular resistance is an alteration in systemic arterial pressure. Therefore basal blood pressure was recorded for K14cre-HIF-α isoform mutants (Fig. 3*A*). Keratinocyte deletion of HIF-1α ($n = 20$) gave rise to a significantly increased systolic (122 mmHg vs. 111 mmHg) and diastolic (98 mmHg vs. 91 mmHg) pressure, i.e., induced hypertension relative to control mice ($n = 34$). In contrast, HIF-2α deletion in keratinocytes ($n = 10$) significantly lowered basal systolic (103 mmHg) and diastolic (82 mmHg) pressures, causing systemic hypotension.

A number of markers of cardiac stress are known to be associated with hypertension. To examine this association more closely, mRNA was isolated from the heart tissue of controls and keratinocyte-deletion HIF-α isoform mutants and was analyzed for the expression of natriuretic peptide A (*Nppa*), natriuretic peptide B (*Nppb*), actin alpha 1 skeletal muscle (*Acta1*), and myosin heavy chain 7 cardiac muscle (*myh7*), a selection of genes recognized to be transcriptionally up-regulated in cardiac tissue from hypertensive subjects (29, 30). All four genes were increased in cardiac tissue from K14cre-HIF-1α mice (Fig. 3*B*), verifying cardiac stress secondary to induced hypertension. Deletion of keratinocyte HIF-2α (Fig. 3*B*) showed a trend toward lowered expression profiles of these same markers in cardiac tissue.

Because cardiac tissue also shows fibrotic changes in hypertension, we examined ventricular walls for fibrosis in mutants and found that fibrotic areas were significantly greater in the hypertensive K14cre-HIF-1α mutants than in controls (Fig. 3*C*). Of note, biochemical analysis of blood samples from K14cre-HIF-1α mice show normal liver and kidney function compared with WT controls (Table S1).

To explore how differential keratinocyte HIF-α isoform expression might influence vascular tension during hypertension, an acute hypertension syndrome was induced in mutant and control mice via 14-d infusion of angiotensin-II (Ang-II) (2 $\mu g \cdot kg^{-1} \cdot min^{-1}$) through a surgically implanted osmotic minipump (31). Mean systolic (158 mmHg vs. 111 mmHg, $P < 0.01$) and diastolic (111 mmHg vs. 89 mmHg, $P < 0.01$) blood pressures were significantly increased at day 14 in Ang-II–treated WT mice as compared with vehicle-treated controls (Fig. S6*A*).

In K14cre-HIF-1α mutant mice ($n = 7$) there was a significant increase in both systolic (187 mm/Hg vs. 170 mm/Hg) and diastolic (138 mmHg vs. 119 mmHg) blood pressures compared with littermate controls (Fig. 4*A*). Here again, the opposite effect on blood pressure was seen in K14cre-HIF-2α mutant mice ($n = 7$), in which substantial protection against Ang-II–induced hypertension was seen, with attenuation in both systolic and diastolic blood pressures (Fig. 4*A*). The percentage of fibrotic cardiac tissue also was significantly less in the K14cre-HIF-2α mutants than in littermate controls (Fig. 4 *B* and *C*). These results indicate that loss of HIF-2α in the skin has an ameliorating effect on the severe hypertension induced in this model.

Analysis of RNA isolated from the skin of K14cre-HIF-1α mice identified no deviation in the expression of NOS2 or arginase-1 or -2 compared with similarly treated (Ang-II) WT controls (Fig. 4*D*). Conversely, K14cre-HIF-2α mice demonstrated a significant increase in NOS2 gene expression (8.01 ± 2.0-fold change, $n = 6$, $P < 0.0.05$) (Fig. 4*D*). This observation was confirmed by a significant increase in skin-associated nitrate concentration (7.8 ± 1 μM vs. 5.0 ± 0.5 μM, respectively, $n = 4$, $P < 0.05$) (Fig. 4*E*). There was a reduction of skin nitrate isolated from K14cre-HIF-1α mice ($n = 4$, $P = 0.06$), again showing an effect opposite that caused by the deletion of the HIF-2α isoform. Of interest, a number of recent studies have documented a heightened interaction/stability of HIF-1α in animals treated with Ang-II (32). We observed a significant and coordinate increase in both HIF-1α and HIF-2α proteins in the skin of WT control mice treated with Ang-II (Fig. 4 *F* and *G*) as well as an increase in the expression of NOS2. The expression of NOS1 mRNA (Fig. S6*B*) and NOS3 protein remained unchanged (Fig. 4*F*).

This last observation indicates that HIF isoform expression is modulated in WT mice by the induction of hypertension. Although this finding is intriguing and clearly supports an essential role for HIF isoform balance in the maintenance of the appropriate peripheral vascular resistance in mice, we wished to determine how this modulation might relate to human hypertensive disease. To ascertain relevance to human hypertension, we recruited consenting subjects that either were normotensive or had established

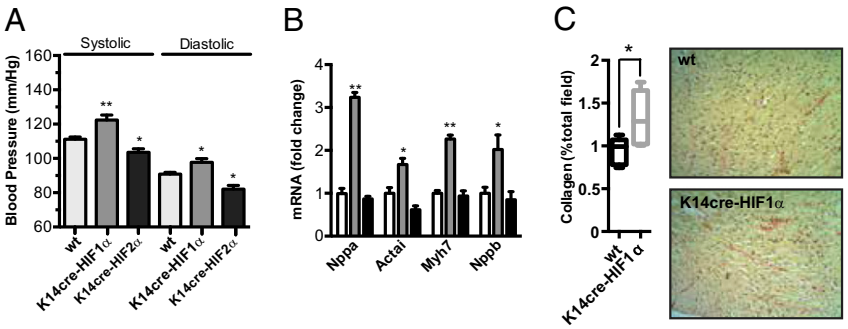

Fig. 3. Murine keratinocyte expression of HIF-1α/-2α subunits modulates systemic blood pressure. (*A*) Blood pressure was measured noninvasively through tail-cuff occlusion. Data are shown as average values of 10 independent readings in 8- to 10-wk-old WT ($n = 34$), K14cre-HIF-1α ($n = 20$), and K14cre-HIF-2α ($n = 10$) mice and are displayed as systolic and diastolic values ± SEM. (*B*) Relative mRNA levels of *Nppa*, *Acta1*, *Myh7*, and *Nppb* (genes known to be influenced by hypertension) in cardiac tissue were determined by qPCR from resting WT (open bar, $n = 3$), K14cre-HIF-1α (gray bar, $n = 3$), and K14cre-HIF-2α (black bar, $n = 3$) mice. (*C*) Baseline cardiac fibrosis was determined in 8- to 10-wk-old K14cre-HIF-1α and WT mice ($n = 5$). Histological sections were stained with Sirius Red, quantified by ImageJ software, and are displayed as percentage of collagen in total fields ± SEM. $*P < 0.05$, $**P < 0.005$.

mild hypertension and who were otherwise healthy as volunteers for skin biopsy analysis of HIF-α expression. Approval for this research was granted by the Cambridge (UK) Research Ethics Committee (Ref:11/EE/0028). Volunteers were screened for hypertension status, age, and medication, as shown in Table S2.

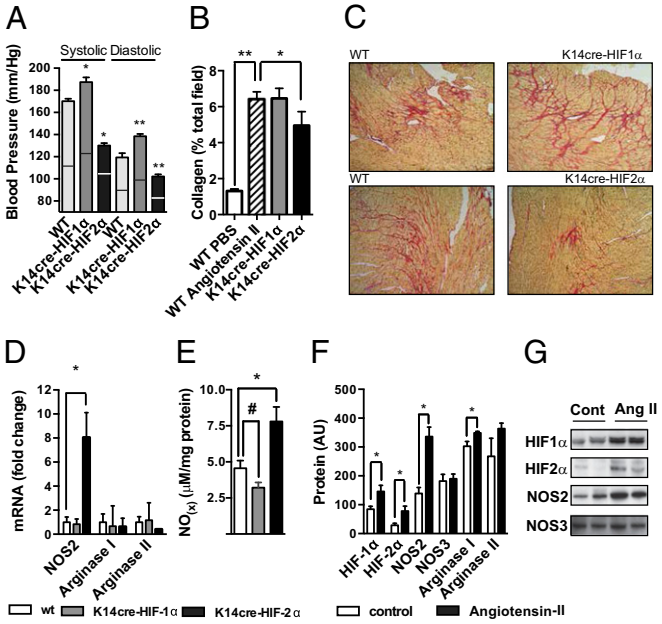

Fig. 4. Epidermal deletion of HIF-2α drives NOS2 expression in skin and reduces cardiac fibrosis in a model of Ang-II–induced hypertension. WT and mutant K14cre mice received a constant infusion of Ang-II (2 $mg \cdot kg^{-1} \cdot d^{-1}$) or vehicle control via an s.c. inserted osmotic pump. (*A*) Blood pressure was measured by tail-cuff occlusion on day 0 (dissecting line) and day14 (bar). Data shown are average values of 10 independent readings from WT ($n = 7$), K14cre-HIF-1α ($n = 7$), and K14cre-HIF-2α ($n = 7$) mice. (*B* and *C*) Cardiac fibrosis was determined in WT, K14cre-HIF-1α ($n = 4$), and K14cre-HIF-2α ($n = 4$) mice 14 d after the insertion of an osmotic pump. (*B*) Histological sections of the left ventricle were stained with Sirius Red and quantified by ImageJ software. (*C*) Representative photomicrographs demonstrate the remarkable contrast in collagen deposition. (*D*) qPCR analysis of *NOS2*, Arginase-I, and Arginase-II mRNA from the skin of WT (open bar, $n = 6$), K14cre-HIF-1α (gray bar, $n = 6$) and K14cre-HIF-2α (closed bar, $n = 6$) mice 14 d after the insertion of an osmotic pump. (*E*) Total nitric oxide was determined in skin lysates by the conversion NOx to NO using a nitric oxide analyzer (Siever). Data are shown as mean ± SEM from WT ($n = 4$), K14cre-HIF-1α ($n = 4$), and K14cre-HIF-2α ($n = 4$) mice 14 d after the insertion of the osmotic pump. (*F*) Protein analysis of skin samples shows an increase in the expression of both HIF-1α and HIF-2α with a corresponding increase of both *NOS2* and arginase-I. Data are shown as mean ± SEM; $n = 4$. (G) Representative photomicrographs of Western blots. $*P < 0.05$, $**P < 0.005$; #p=0.06.

Initial blood pressure measurements confirmed the hypertensive state of the subjects, with significantly higher systolic (154 mm/Hg vs. 126 mm/Hg, $P < 0.005$), diastolic (89 mmHg vs. 73 mmHg, $P < 0.005$), and mean arterial (110 mm/Hg vs. 91 mm/Hg, $P < 0.005$) blood pressures in the hypertensive group ($n = 16$) than in healthy normal controls ($n = 24$) (Fig. 5*A*). A determination of nitrate levels in these subjects showed that hypertension also was correlated with a significantly decreased amount of skin nitrate (Fig. 5*B*) with a strong trend toward a reduction in NOS2 gene expression (Fig. S7) Immunohistochemical analysis of epidermal expression of the HIF-α isoform showed that decreased expression of HIF-1α in the epidermal layer correlated significantly with increased mean blood pressure, whereas increased epidermal HIF-2α expression, specifically nuclear localization of HIF-2α, correlated very significantly with increased mean blood pressure. These data again suggest that the HIFα isoforms have opposing roles in regulating peripheral vascular resistance and, ultimately, blood pressure (Fig. 5 *C* and *D*).

Discussion

The distribution of blood flow through vascular beds is regulated through complex adjustments of the vascular tone and thus the resistance of the microcirculation to blood flow. HIF-α isoforms are expressed in a wide range of tissue types, and, as oxygen-responsive modulators of vascular function, they act as agents that respond to different levels of tissue perfusion. The two main HIF-α factors have a number of both overlapping and divergent gene targets, but recent evidence has indicated that they can act to coregulate important biological control pathways through functionally oppositional targets. Here we report evidence that a balance of HIF-1α and HIF-2α in the skin is essential for controlling peripheral vascular resistance. Previously we have shown that inflammatory cytokines can influence the balance of HIF-1α and HIF-2α, and that this balance in turn regulates macrophage production of NO via differential regulation of the HIF target genes iNOS/NOS2 and arginase1 (22). Our data indicate that this pathway for control of NO homeostasis also exists in keratinocytes, although in this case in the absence of cytokine regulation. In this peripheral and highly vascularized tissue, it is a localized mechanism for control of vascular flow. Because NOS2 regulation differs between mice and men, it will be important to follow up with a more detailed examination of HIF-dependent NOS2 regulation in human peripheral vasculature (33).

Vasodilation induced by nitric oxide is known to act as a physiological counterbalance to the vasoconstriction controlled by both the sympathetic nervous system and by renin-angiotensin action. It is clear that NO is a key regulator of peripheral vascular resistance: Blockade of NO synthesis with inhibitory L-arginine analogs has been shown to increase peripheral vasoconstriction (34, 35) and increase systemic blood pressure (34, 36). A number of studies also have linked NO bioavailability with endothelial cell dysfunction and hypertension (37, 38). Hypertensive subjects have lower serum levels of bioavailable NO than normotensive controls (38, 39), and increasing the availability of L-arginine, the natural substrate

PHYSIOLOGY

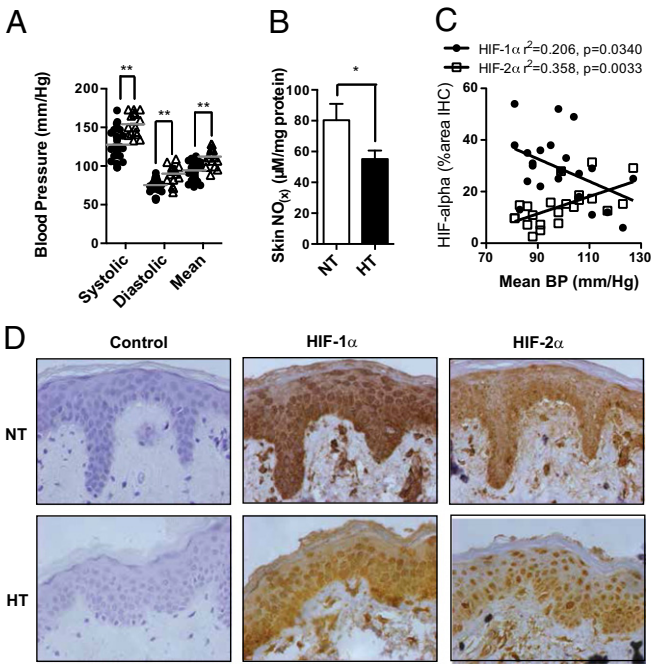

Fig. 5. Expression pattern of HIF-1α and HIF-2α in the skin of normotensive and hypertensive subjects. (*A*) Sphygmomanometer measurements of volunteers' blood pressure. Normotensive (●, $n = 24$) and hypertensive (△, $n = 16$) dot plots are divided into systolic, diastolic, and arterial mean blood pressure. $^{**}P < 0.005$. (*B*) Total NO was determined in skin lysates by the conversion of NOx to NO using a nitric oxide analyzer (Siever). Data are shown as mean ± SEM. Normotensives (NT, $n = 17$) are shown by the open bar, and hypertensive subjects (HT, $n = 10$) are shown as the closed bar. $^{*}P < 0.05$,). (*C*) Linear regression analysis of the immunohistochemistry (the percentage positive signal in the squamous epithelial layer) of human skin stained for HIF-1α or HIF-2α plotted against the mean BP (mmHg). HIF-1α (●, $n = 22$) produced a significant correlation ($r^2 = 0.2057$, $P = 0.0340$). HIF-2α (□, $n = 22$) also produced a significant correlation ($r^2 = 0.3580$, $P = 0.0033$). (*D*) Histological analysis. Shown are representative photomicrographs of HIF-1α and HIF-2α expression in human skin.

of NOS, leads to heightened vasodilation and decreases in arterial blood pressure (40, 41).

Increased peripheral vascular resistance in the skin can lead to alterations in vascular density and ultimately to vascular rarefaction. The arginase enzymes, which are shown here to be induced by HIF-2α, are important not only because they can influence NO generation indirectly, but also because they are critical in channeling L-arginine to L-ornithine and, ultimately, for the production of the polyamines and L-proline. These in turn contribute to increased collagen synthesis, which itself is linked to fibrosis. Thus, an aberrant spectrum of HIF isoform function/expression may underlie many of the fibrotic vascular pathologies evident in patients with hypertension.

These data show that hypertensive individuals differentially express HIF-1α and HIF-2α, with a loss of the concordant regulation evident in normotensives. We demonstrated previously that deletion of the HIF negative regulator VHL in keratinocytes can disturb vascular flow to other organs, including to the viscera (12). This alteration in vascular flow has striking physiological effects, including changes in the synthesis of erythropoietin at distant sites. Clearly, the overall regulation of NO homeostasis in tissue beds via oxygen-responsive factors is a potent mechanism for achieving physiological balance, apart from the traditional axes of this control such as the kidney and central nervous system. Previous studies by Prabhakar and co-workers (19, 21) reported that hemizygous global deletion of HIFα isoforms did not cause hypertension when HIF-1α was reduced but did cause hypertension in global HIF-2α hemizygotes. These results, in contrast with those shown here, point out the critical importance of considering the role of these factors in a tissue-specific context. Hypertension involves peripheral vascular resistance, and the resistance and resultant vascular remodeling in the periphery will cause compensatory changes in other vascular beds. A global deletion will show this compensation in a time- and tissue-dependent manner that will be different from that engendered by deletion in a single tissue type, as here. Both types of experimental observation are crucial for a better understanding of the complexity of hypertension and the role of the HIFs in its etiology.

Materials and Methods

Animals. All animals were housed in a facility approved by the International Association for the Assessment and Accreditation of Laboratory Animal Care, and animal experiments were conducted in accordance with the National Institutes of Health *Guide for the Care and Use of Laboratory Animals* (42).

Targeted deletion of HIF-1α and HIF-2α in keratinocytes was created by crossing mice (C57Bl6/j) homozygous for the floxed allele in HIF-1α, HIF-2α, or VHL into a background of Cre recombinase expression driven by the K14 promoter, which is specific to cells of the keratinocyte linage.

Metabolic Analysis. Energy expenditure of the K14-mutant mice and their WT littermates was measured using the Columbus Instruments Oxymax system according to the manufacturer's instructions. For exercise tolerance testing, mice were allowed to acclimatize to the enclosed treadmill environment for 15 min before stimulation. The treadmill was initiated at 5 M/min increasing to 9, 12, 15, and 18 M/min on a 15° incline. VO_2 was measured every 30 s on a 150-s cycle before the speed of the treadmill was increased.

Mouse Temperatures and Blood Pressure Analysis. Surface temperatures were measured with a FLIR Thermovision A20 thermal infrared camera, and image data were analyzed using FLIR image analysis software. All core body temperatures were taken rectally with a TEGRAM 871A digital thermometer (Braintree Scientific Inc) using a RET-1 rectal probe. Temperature acclimation tests were conducted in bare cages with water and food supplied ad libitum. Rectal temperatures were taken before and every hour for 6 h during the temperature acclimation test. Blood pressure was monitored in restrained conscious mice by the tail-cuff occlusion method, according to the manufacturer's instructions (Coda system; Kent Scientific). This method of blood pressure analysis has been validated extensively. Repeat measurements using tail-cuff occlusion have been shown to match radio telemetry analysis closely (43).

Immunofluorescence and Quantification of Vascular Density and Vascular Diameter. Mouse skin isolated from WT and K14cre animals was frozen in OCT (Tissue-Tek). Staining for the epidermal basal layer markers K5, MAC-1, CD31 (BD PharMingen) was performed on 8-μm frozen sections after the tissues were fixed for 10 min in 4% (wt/vol) paraformaldehyde or acetone (for CD31). Images were acquired on an Olympus Bx51 microscope with an Olympus DP70 camera. Acquisition was performed using a 40× 1.3 UPlan FL N objective (Olympus). For quantitation of vascular density in the skin, CD31 staining was calculated as a percentage of dermal area by ImageJ software (National Institutes of Health). Results are from five random fields using a 10× objective and normalized against the WT value. To assess vessel diameter, confocal microscopic images of the skin were acquired using a LSM 700 laser scanning microscope fitted with an Axio Observer.Z1 (Carl Zeiss). The blood vessels were examined only in an area of the dermis within 100 mm of the epiderma–dermal junction. The diameters of blood vessels were measured by ImageJ software. Results are from five random fields using a 40× objective.

Cardiac Fibrosis Analysis. Formalin-fixed, paraffin wax-embedded hearts were sectioned (4 μm), and collagen deposition was assessed on Sirius Red-stained sections. Image analysis was performed using ImageJ software.

RNA Analysis. Total RNA was isolated from skin, lung, heart, and liver using TRI-reagent (Sigma) followed by RNA clean-up and DNase digest using RNeasy column kits (Qiagen). First-strand synthesis was performed with 1μg of total RNA using a high-capacity cDNA kit (Applied Biosystems) according to the manufacturer's instructions. Relative gene expression was determined by quantitative PCR (qPCR) (ABI Prism 7700 sequence detection system; Applied Biosystems) and was amplified in SYBR-Green master mix (Applied Biosystems) and relevant primers from Qiagen. Relative gene-expression levels were related to β-actin using the 2CT method. Relative gene-expression levels in human skin were related to YWHAZ expression.

Immunoblotting. Tissue samples were lysed in RIPA buffer. A total of 50 μg of whole-cell lysates were loaded on to a 4–12% Bis-Tris gel from Invitrogen (NuPAGE). The primary antibodies used in this study were rabbit polyclonal anti–HIF-1α anti–HIF-2α (1:1,000; Novus Biologicals), anti-NOS2, anti-NOS3, anti–arginase-II (1:200; Santa Cruz Biotechnology), and mouse monoclonal anti–arginase-I (1:1,000,; Santa Cruz Biotechnology). Secondary antibodies used were goat anti-rabbit IgG-HRP (1:2,000; R&D Systems) and rabbit anti-mouse IgG-HRP (1:5,000; GE Healthcare).

Nitric Oxide Analysis. Blood samples were centrifuged to separate plasma and were passed through a column with a 10-kDa cutoff filter. Skin nitrogen oxides (NO_x) were isolated from 500 mg of homogenized tissue using a hypotonic lysis buffer and were centrifuged at 1,000 × *g*, 4 °C, for 5 min. All samples were analyzed for total NO_x content using an NOA 280i (Siever, GE Healthcare) according to the manufacturer's instructions.

Model of Ang-II–Induced Hypertension. Ang-II or vehicle control was administered through an osmotic minipump (Model 2002; Alzet) implanted s.c. to deliver 2 $\mu g \cdot kg^{-1} \cdot min^{-1}$ over a 14-d period.

Human Skin Biopsy. Small elliptical skin biopsies were removed carefully from the lateral abdominal wall of 33 consenting healthy volunteers at the Addenbrooke's University of Cambridge teaching Hospital NHS Foundation Trust, Cambridge, UK following a protocol approved by the Cambridge (UK) Research Ethics Committee (Ref:11/EE/0028). Participants consisted of 16 subjects with previously diagnosed mild hypertension and 17 normotensive subjects. The relevant participant details are presented in Table S1. All skin biopsy samples collected were divided into two parts and were rapidly snap frozen in liquid nitrogen for RNA and protein analysis.

Human Skin Immunohistochemistry. Formalin-fixed, paraffin wax-embedded skin biopsies were sectioned (4 μm) and incubated with monoclonal mouse anti-human HIF1α (1:100) and polyclonal rabbit anti-human HIF2α (1:200) (both from Novus Biologicals). Antibodies were detected using 3,3′-diaminobenzidine tetrahydrochloride to create a brown reaction product, counterstained with hematoxylin (Dako, and examined by light microscopy. Quantification was performed by ImageJ software.

Statistic Analysis. All data represent the mean (± SEM) of *n* separate experiments unless otherwise stated. Differences between groups were assessed using a *t* test unless otherwise stated. A *P* value of <0.05 was considered significant.

ACKNOWLEDGMENTS. This work was funded by Cambridge National Institute for Health Research Biomedical Research Center, Papworth Hospital National Health Service trust, The Wellcome Trust (Grant WT092738MA), and the US National Institutes of Health (Grants 5R01AI093451, 1R01AI096852, and 5R01CA153983).

1. Duling BR, Klitzman B (1980) Local control of microvascular function: Role in tissue oxygen supply. *Annu Rev Physiol* 42:373–382.
2. Stewart J, et al. (2004) Noninvasive interrogation of microvasculature for signs of endothelial dysfunction in patients with chronic renal failure. *Am J Physiol Heart Circ Physiol* 287(6):H2687–H2696.
3. Khan F, Litchfield SJ, Stonebridge PA, Belch JJ (1999) Lipid-lowering and skin vascular responses in patients with hypercholesterolaemia and peripheral arterial obstructive disease. *Vasc Med* 4(4):233–238.
4. Rossi M, Carpi A (2004) Skin microcirculation in peripheral arterial obliterative disease. *Biomed Pharmacother* 58(8):427–431.
5. Green DJ, et al. (2006) Impaired skin blood flow response to environmental heating in chronic heart failure. *Eur Heart J* 27(3):338–343.
6. De Ciuceis C, et al. (2007) Structural alterations of subcutaneous small-resistance arteries may predict major cardiovascular events in patients with hypertension. *Am J Hypertens* 20(8):846–852.
7. Noon JP, et al. (1997) Impaired microvascular dilatation and capillary rarefaction in young adults with a predisposition to high blood pressure. *J Clin Invest* 99(8): 1873–1879.
8. Semenza GL (2007) Oxygen-dependent regulation of mitochondrial respiration by hypoxia-inducible factor 1. *Biochem J* 405(1):1–9.
9. Pouysségur J, Dayan F, Mazure NM (2006) Hypoxia signalling in cancer and approaches to enforce tumour regression. *Nature* 441(7092):437–443.
10. Semenza GL (2003) Targeting HIF-1 for cancer therapy. *Nat Rev Cancer* 3(10):721–732.
11. Gordan JD, Bertout JA, Hu CJ, Diehl JA, Simon MC (2007) HIF-2alpha promotes hypoxic cell proliferation by enhancing c-myc transcriptional activity. *Cancer Cell* 11(4): 335–347.
12. Boutin AT, et al. (2008) Epidermal sensing of oxygen is essential for systemic hypoxic response. *Cell* 133(2):223–234.
13. Dang CV, Kim JW, Gao P, Yustein J (2008) The interplay between MYC and HIF in cancer. *Nat Rev Cancer* 8(1):51–56.
14. Ravi R, et al. (2000) Regulation of tumor angiogenesis by p53-induced degradation of hypoxia-inducible factor 1alpha. *Genes Dev* 14(1):34–44.
15. Bertout JA, et al. (2009) HIF2alpha inhibition promotes p53 pathway activity, tumor cell death, and radiation responses. *Proc Natl Acad Sci USA* 106(34):14391–14396.
16. Roberts AM, et al. (2009) Suppression of hypoxia-inducible factor 2alpha restores p53 activity via Hdm2 and reverses chemoresistance of renal carcinoma cells. *Cancer Res* 69(23):9056–9064.
17. Brugarolas J, et al. (2004) Regulation of mTOR function in response to hypoxia by REDD1 and the TSC1/TSC2 tumor suppressor complex. *Genes Dev* 18(23):2893–2904.
18. Kline DD, Peng YJ, Manalo DJ, Semenza GL, Prabhakar NR (2002) Defective carotid body function and impaired ventilatory responses to chronic hypoxia in mice partially deficient for hypoxia-inducible factor 1 alpha. *Proc Natl Acad Sci USA* 99(2):821–826.
19. Peng YJ, et al. (2011) Hypoxia-inducible factor 2α (HIF-2α) heterozygous-null mice exhibit exaggerated carotid body sensitivity to hypoxia, breathing instability, and hypertension. *Proc Natl Acad Sci USA* 108(7):3065–3070.
20. Nanduri J, et al. (2009) Intermittent hypoxia degrades HIF-2alpha via calpains resulting in oxidative stress: Implications for recurrent apnea-induced morbidities. *Proc Natl Acad Sci USA* 106(4):1199–1204.
21. Yuan G, et al. (2013) Mutual antagonism between hypoxia-inducible factors 1α and 2α regulates oxygen sensing and cardio-respiratory homeostasis. *Proc Natl Acad Sci USA* 110(19):E1788–E1796.
22. Takeda N, et al. (2010) Differential activation and antagonistic function of HIF-alpha isoforms in macrophages are essential for NO homeostasis. *Genes Dev* 24(5):491–501.
23. Boegehold MA (2010) Endothelium-dependent control of vascular tone during early postnatal and juvenile growth. *Microcirculation* 17(5):394–406.
24. Qiu C, Muchant D, Beierwaltes WH, Racusen L, Baylis C (1998) Evolution of chronic nitric oxide inhibition hypertension: Relationship to renal function. *Hypertension* 31(1):21–26.
25. Nagai M, et al. (2011) Role of blood cell-associated angiotensin II type 1 receptors in the cerebral microvascular response to ischemic stroke during angiotensin-induced hypertension. *Exp Transl Stroke Med* 3:15.
26. Munder M, Eichmann K, Modolell M (1998) Alternative metabolic states in murine macrophages reflected by the nitric oxide synthase/arginase balance: Competitive regulation by CD4+ T cells correlates with Th1/Th2 phenotype. *J Immunol* 160(11): 5347–5354.
27. Melillo G, et al. (1995) A hypoxia-responsive element mediates a novel pathway of activation of the inducible nitric oxide synthase promoter. *J Exp Med* 182(6):1683–1693.
28. Carter R, 3rd, Wilson TE, Watenpaugh DE, Smith ML, Crandall CG (2002) Effects of mode of exercise recovery on thermoregulatory and cardiovascular responses. *J Appl Physiol* 93(6):1918–1924.
29. Marques FZ, Campain AE, Yang YH, Morris BJ (2010) Meta-analysis of genome-wide gene expression differences in onset and maintenance phases of genetic hypertension. *Hypertension* 56(2):319–324.
30. Ye P, West MJ (2003) Cosegregation analysis of natriuretic peptide genes and blood pressure in the spontaneously hypertensive rat. *Clin Exp Pharmacol Physiol* 30(12): 930–936.
31. Vital SA, Terao S, Nagai M, Granger DN (2010) Mechanisms underlying the cerebral microvascular responses to angiotensin II-induced hypertension. *Microcirculation* 17(8):641–649.
32. Sanchez-Lopez E, et al. (2005) Angiotensin II regulates vascular endothelial growth factor via hypoxia-inducible factor-1alpha induction and redox mechanisms in the kidney. Antioxidants & redox signaling 7(9-10):1275-1284.
33. Vitek MP, et al. (2006) Characterization of NO and cytokine production in immune-activated microglia and peritoneal macrophages derived from a mouse model expressing the human NOS2 gene on a mouse NOS2 knockout background. Antioxidants & redox signaling 8(5-6):893-901.
34. Vecchione C, et al. (2009) Pressure-induced vascular oxidative stress is mediated through activation of integrin-linked kinase 1/betaPIX/Rac-1 pathway. *Hypertension* 54(5):1028–1034.
35. Qiu C, Engels K, Samsell L, Baylis C (1995) Renal effects of acute amino acid infusion in hypertension induced by chronic nitric oxide blockade. *Hypertension* 25(1):61–66.
36. Vecchione C, et al. (2005) Protection from angiotensin II-mediated vasculotoxic and hypertensive response in mice lacking PI3Kgamma. *J Exp Med* 201(8):1217–1228.
37. Mason RP, et al. (2009) Loss of arterial and renal nitric oxide bioavailability in hypertensive rats with diabetes: Effect of beta-blockers. *Am J Hypertens* 22(11):1160–1166.
38. Hermann M, Flammer A, Lüscher TF (2006) Nitric oxide in hypertension. *J Clin Hypertens (Greenwich)* 8(12, Suppl 4):17–29.
39. Ghasemi A, Zahediasl S, Syedmoradi L, Azizi F (2011) Association between serum nitric oxide metabolites and hypertension in a general population. *Int Angiol* 30(4):380–387.
40. Dong JY, et al. (2011) Effect of oral L-arginine supplementation on blood pressure: A meta-analysis of randomized, double-blind, placebo-controlled trials. *Am Heart J* 162(6):959–965.
41. Gokce N (2004) L-arginine and hypertension. *J Nutr* 134(10 Suppl):2807S–2811S; discussion 2818S–2819S.
42. Committee on Care and Use of Laboratory Animals (1985) *Guide for the Care and Use of Laboratory Animals* (Natl Inst Health, Bethesda), DHHS Publ No (NIH) 85-23.
43. Feng M, et al. (2008) Validation of volume-pressure recording tail-cuff blood pressure measurements. *Am J Hypertens* 21(12):1288–1291.